等离子熔射过程中射流与粒子流的加热效应

夏 卫生[1]，　张海鸥[2]，　王桂兰[1]，　杨云珍[1]，　邹　阳[1]

（1. 华中科技大学 材料成形与模具技术国家重点实验室，武汉　430074；
2. 华中科技大学 数字制造与装备技术国家重点实验室，武汉　430074）

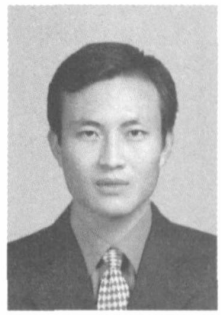

夏 卫生

摘　要：采用 CCD 图像采集系统与图像处理技术提取等离子射流长度；以红外测温仪检测的单位时间内基体温度变化来衡量加热效应，研究不同熔射距离与射流长度条件下射流和粉末粒子流对基体的加热效应特点。结果表明，当熔射距离不大于射流长度时，基体温升主要来至于射流加热效应；随着熔射距离增大，射流对基体的加热效应迅速减弱；当熔射距离大于射流长度时，粒子流加热效应比较明显。提出射流长度可以作为合理选择熔射距离的特征评价指标，并通过不同熔射距离条件下熔射皮膜的截面尺寸以及形貌进行验证。

关键词：等离子熔射；加热效应；射流；粒子流；射流长度；熔射距离

中图分类号：TG174.442　　文献标识码：A　　文章编号：0253－360X(2007)11－029－04

0　序　　言

等离子熔射过程中基体与皮膜温升主要来源于等离子射流和粉末粒子流的加热效应，而温度变化是决定熔射皮膜的成形性和质量的重要因素。虽然相关文献对射流与基体之间传热过程分别进行了试验与模拟研究[1－6]，但是均没有涉及到如何根据射流长度来确定热传递方式，而且只有较少文献考虑了粉末粒子的加热效应。如何控制射流和粒子流对基体与皮膜的加热效应[7]，从而达到控制基体和皮膜温度均匀分布，进而保证熔射成形性和皮膜质量是等离子熔射过程控制的关键与难题之一[8,9]。

借助过程检测手段获取不同工艺条件下等离子射流长度，据此区分射流和粒子流对基体的加热效应特点以及选择合理熔射距离尚未见相关研究报道。作者首先采用 CCD 图像采集系统与图像处理技术提取等离子射流长度，用红外测温仪检测单位时间内基体温度变化来衡量加热效应。然后对比分析不同熔射距离（H）与射流长度条件下射流、粒子流的加热效应，从而为合理熔射工艺制定提供依据。

1　试　　验

1.1　等离子熔射试验条件

基体材料为 45 钢，表面经除锈、打毛处理，熔射前用丙酮清洗。采用内送粉方式输送镍基合金粉末 ZX.Ni45 进行熔射，等离子喷枪的喷嘴直径为 ϕ8 mm。采用 Ar－N_2 作为等离子体工作气体，其中 Ar 气体流速为 20 L/min，压力为 0.6 MPa；N_2 气体流速为 10 L/min，压力为 0.4 MPa。其它工艺参数见表 1。

表 1　等离子熔射工艺参数

Table 1　Parameters setting during plasma spraying

焊接电流 I/A	电弧电压 U/V	送粉量 P/(g·s^{-1})	熔射距离 H/mm	环境温度 T/℃	送粉口直径 D/mm
400	50	0.076	100/150/200/250	20.5	2

1.2　射流图像处理与射流长度确定

等离子射流长度提取流程如图 1 所示。用 CCD 采集射流图像，通过滤波去噪、图像二值化和边缘提取等处理方法获取射流形貌[10]。射流长度通过基于照相原理进行标定的图像尺寸与标尺长度之间对应关系求得。用该方法得到表 1 工艺参数对应的射流长度为195 mm，因此设定熔射距离分别为 100，

收稿日期：2007－02－06
基金项目：国家自然科学基金资助项目（50475134，50675081）

150, 200 和250 mm。

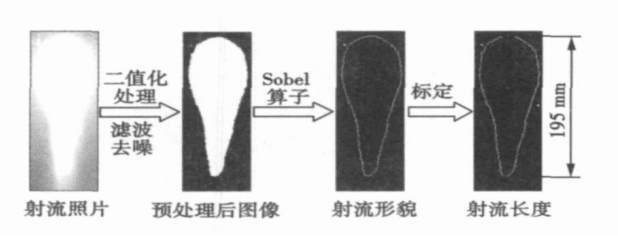

图 1 等离子射流长度提取流程

Fig. 1 Processing flowchart for length of plasma jet

1.3 加热效应的测量

采用美国雷泰公司 Thermalert TX 系列 LT 型红外测温仪进行温度检测, 其响应时间为 165 ms, 光学分辨率为 33∶1。红外测温仪工作波段为 8 ~ 14 μm, 可以避免等离子熔射现场气氛和等离子体辐射的干扰[11, 12]。设定基体发射率为0.95, 皮膜发射率为0.85。

加热效应测量原理如图 2 所示。固定等离子熔射工艺参数, 利用射流与粉末粒子流分别对基体进行定点加热。在距离等离子喷枪中心线与基体交点10 mm处, 用红外测温仪检测基体温度, 通过被检测点的温度变化来衡量加热效应。检测时间设定3 min或者温度达到红外测温仪的测温上限300 ℃。

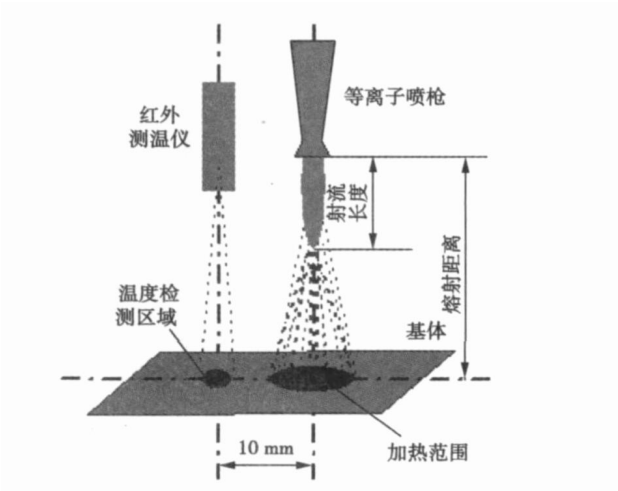

图 2 加热效应测量示意图

Fig. 2 Diagrammatic sketch for measurement of heating effect

2 试验结果与分析

2.1 熔射距离对射流加热效应影响

在不同熔射距离条件下, 基体温度随时间变化曲线如图 3 所示。由图可知, 当熔射距离 H 为100 mm时基体温度迅速升高, 在116 s时达到300 ℃。熔射距离 H 调整为150 mm时温升较快, 在180 s时最终温度达到263.4 ℃。但是熔射距离 H 为250 mm时, 最终温度只有138.2 ℃。可见熔射距离对射流加热效应有着决定性的影响, 熔射距离的增加将会导致等离子射流对基体的加热热流急速下降。熔射距离大于和小于射流长度50 mm, 对应温度曲线与熔射距离接近射流长度时的温度曲线差值相差不大。

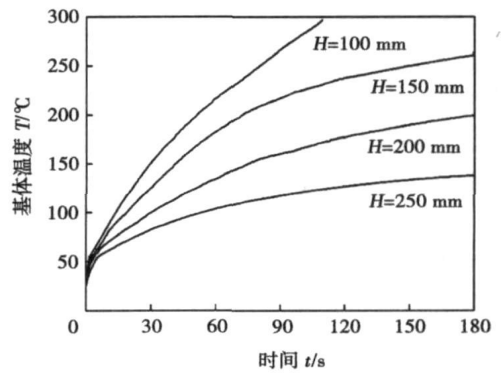

图 3 熔射距离变化对射流加热效应影响

Fig. 3 Influence of spraying distance on heating effect of plasma jet

2.2 熔射距离对粒子流加热效应影响

不同熔射距离条件下基体温度随粒子流作用时间变化曲线如图 4 所示。图中除熔射距离为100 mm对应的温度曲线之外, 其余温度曲线由于熔射过程中皮膜出现翘曲、剥落等破坏现象均有波动。当皮膜破坏发生时, 皮膜与基体不能紧密接触, 其吸收热量不能及时与基体之间通过热传导散失, 所以皮膜温度会出现陡升现象。

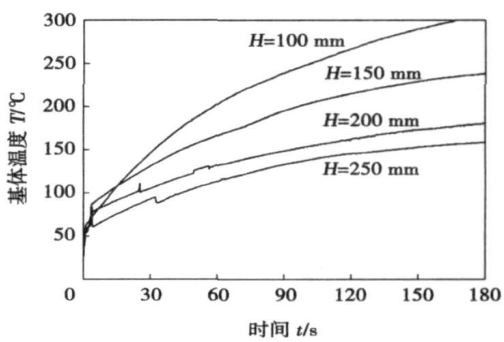

图 4 熔射距离变化对粒子流加热效应影响

Fig. 4 Influence of spray distance on the heating effect of particle flux

熔射距离为100 mm时能够有效沉积, 但温升较快, 在 166 s 时上升至 300 ℃。熔射距离分别为

200 mm和250 mm对应的两条温度曲线基本相差20 ℃，而熔射距离为150 mm对应温度曲线却比距离为200 mm温度曲线高50 ℃左右。可见由于粉末粒子携带热量传递到基体和皮膜上的影响，导致不同熔射距离对应温度差值并不均匀，与图 3 中射流加热效应特点不同。

2.3　熔射距离对加热效应影响的比较

不同熔射距离条件下射流和粒子流加热效应对比如图5 所示。总体来说，熔射刚开始时，粒子流加热效应要强于射流作用。因为粒子对基体的加热效应更加集中[7]。当熔射距离小于射流长度时，射流加热效应作用下温度变化曲线的最终温升均高于粒子流加热效应作用曲线，熔射距离为 150 mm 时两条曲线最终温度相差25.2 ℃。因为当熔射距离小于射流长度时，等离子射流直接冲击到基体表面，在喷枪中心线与基体交点附近形成一个能够进行强热流交互的滞止区。局部过高的换热强度引起基体温度迅速上升[4, 13]。送粉后部分射流能量用于粉末粒子加热，反而降低了射流加热效应。当熔射距离接近于射流长度时，与从图 5 中得出的熔射距离小于射流长度时的结论完全吻合。

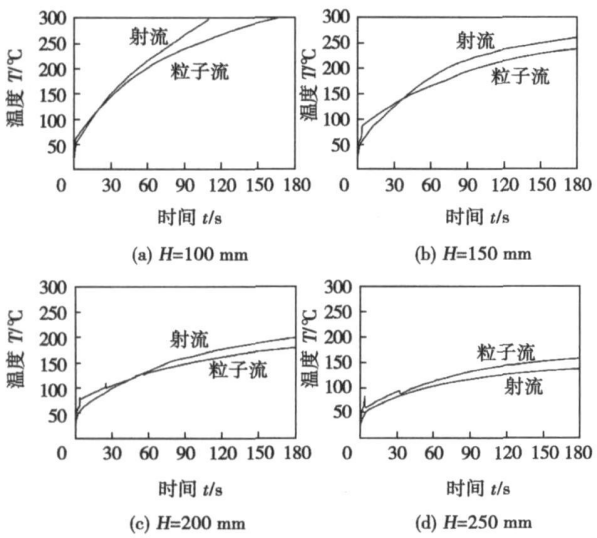

图 5　不同熔射距离条件下射流和粒子流加热效应对比

Fig. 5　Comparison of heating effect between plasma jet and particle flux under different spraying distances

当熔射距离大于射流长度时，从图 5 可以看出，粒子流加热效应强于射流，粒子流作用温度曲线对应最终温升要高于射流作用对应温升19.9 ℃。因为冲击到基体和已熔射皮膜上的粉末粒子携带热量传递到基体上，导致局部粒子沉积区域温度上升，而且射流对基体加热效应明显减弱，所以最终粒子流加热效应要强于射流加热效应。

3　合理熔射距离范围选择

图 6 为不同熔射距离对应的皮膜截面厚度分布。由图可知，熔射距离为100 mm时，皮膜厚度分布比较对称。但是随着熔射距离增加，粒子沉积区域发散，沉积厚度下降。图 7 为不同熔射距离条件下皮膜形貌。从图 7a 中可以看出，当熔射距离为100 mm时，皮膜与基体紧密结合；但是镍基合金皮膜表面呈灰色，基体与已熔射皮膜表面氧化比较严重（因为熔射材料为合金粉末，对陶瓷粉末不会发生该现象）。当熔射距离为150 mm时，有着较好的成形性和形成厚皮膜能力，并且皮膜较亮（图 7b），因此该熔射距离适合于该组工艺条件下等离子熔射。当熔射距离接近于射流长度时，皮膜易从基体表面脱落（图 7c）。将熔射距离增加到250 mm时，整个熔射过程中由于结合力差只能形成0.02～0.03 mm薄层（图 7d），但是此时基体温升较小，因此可以用于采用等离子喷枪进行基体预热过程中，保证预热过程温升较小从而避免在基体表面形成厚氧化层。

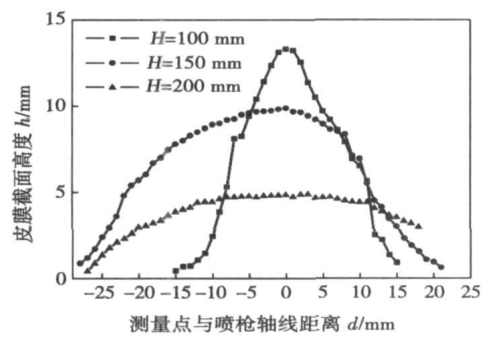

图 6　不同熔射距离条件下皮膜截面厚度分布

Fig. 6　Cross－section thickness profiles of deposited coatings under different spraying distances

综上所述，可以通过以下方式选取合理熔射距离参数。

（1）首先确定相关工艺条件下射流长度。

（2）预热过程中熔射距离的选择。熔射距离应大于射流长度，但是不能太大，否则需要较长时间才能将基体加热到合理临界温度，同时射流长时间作用反而会使金属基体表面形成较厚的氧化层[14]。

（3）熔射过程中熔射距离的选取。一般来说，熔射距离应小于射流长度。对熔点较低的粉末或者粒度较小的纳米、超细粉末，应当采用较小的熔射距离，避免粉末粒子在射流中停留时间过长，导致粉末

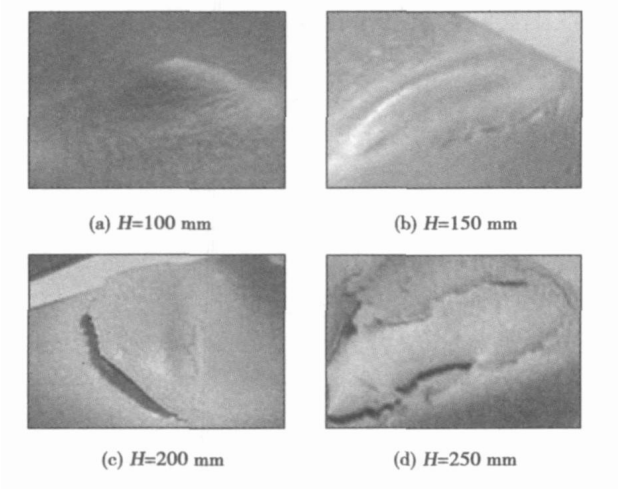

图 7 不同熔射距离条件下皮膜形貌

Fig. 7 Appearance of deposited coatings under different spraying distances

气化；对熔点较高的陶瓷粉末则可以适当提高熔射距离，从而提高粒子飞行速度，提高与基体之间的结合力与沉积效率。然而由于熔射距离影响粉末粒子在射流中停留时间，从而影响粒子飞行特征参数（粒子温度、速度、流量等）。因此结合不同类型粉末粒子的飞行特征参数检测结果，即可选出最优的熔射距离，以期获得尽可能高的粒子表面温度和速度[15]。

4 结 论

（1）当熔射距离小于或等于射流长度时，基体温升取决于射流加热效应。送粉之后由于部分射流能量用于粉末粒子加热，反而降低了射流加热效应。随着熔射距离增大，射流加热效应迅速减弱。

（2）当熔射距离大于射流长度时，粒子流加热效应比较明显，射流加热效应相对减弱，适用于基体预热。

（3）结合射流长度能够确定预热和熔射工艺中熔射距离的合理选择范围，从而降低甚至控制到基体与皮膜的热传递，不需考虑现场环境与设备等外部因素的影响。

参考文献：

[1] Martin H. Heat exchanger design handbook [M]. New York: Begell House, 1998.

[2] Fauchais P, Vardelle A. Heat mass and momentum transfer in coating formation by plasma spraying [J]. International Journal of Thermal Sciences, 2000, 39(9—11): 852—870.

[3] Bolot R, Imbert M, Coddet C. On the use of a low-reynolds extension to the Chen-Kim (K-epsilon) model to predict thermal exchanges in the case of an impinging plasma jet [J]. Journal of Heat and Mass Transfer: 2001, 44(6): 1095—1106.

[4] Bolot R, Coddet C, Imbert M, *et al*. Mathematical modeling of a plasma jet impinging on a flat structure [C] // Thermal Spray: Meeting the Challenges of the 21st Century. ASM International. USA: Materials Park. OH, 1998: 439—444.

[5] Bao Y, Gawne D T, Zhang T. Computational model for the prediction of the temperatures in the coating during thermal spray [C] // Thermal Spray 2004: Advances in Technology and Application. ASM International. USA: Materials Park. OH, 2004: 730—735.

[6] Bao Y, Zhang T, Gawne D T. Non-steady state heating of substrate and coating during thermal-spray deposition [J]. Surface and Coatings Technology, 2005, 194(1): 82—90.

[7] Bolot R, Li L, Bonnet R, *et al*. Modeling of the substrate temperature evolution during the APS thermal spray process [C] // Thermal Spray 2003: Advancing the Science and Applying the Technology. ASM International. USA: Materials Park. OH, 2003: 949—954.

[8] Moreau C. Towards a better control of thermal spray process [C] // Thermal Spray: Meeting the Challenges of the 21st Century. ASM International. USA: Materials Park. OH, 1998: 1681—1693.

[9] Fauchais P. Understanding plasma spraying [J]. Journal of Physics D: Applied Physics, 2004, 37(9): R86—R108.

[10] 张海鸥，刘 韵，王桂兰，等. 基于模式识别的等离子射流形态特征研究 [J]. 机械科学与技术，2006，25(12)：1476—1479.

[11] Friedrich C J, Gadow R, Killinger A, *et al*. IR thermographic imaging-a powerful tool for on-line process control of thermal spraying [C] // Thermal Spray 2001: New Surfaces for a New Millennium. ASM International. USA: Materials Park. OH, 2001: 779—786.

[12] Fauchais P, Montavon G, Vardelle M, *et al*. Developments in direct current plasma spraying [J]. Surface and Coatings Technology, 2006, 201(5): 1908—1921.

[13] 杨世铭，杨文铨. 传热学[M]. 北京：高等教育出版社，1998.

[14] Bianchi L, Baradel N, Liorca I N, *et al*. Influence of plasma spraying parameters on coating damage [C] // Thermal Spray: Surface Engineering via Applied Research. ASM International. USA: Materials Park. OH, 2000: 29—36.

[15] Fincke J R, Swank W D, Bewley R L, *et al*. Diagnostics and control in the thermal spray process [J]. Surface and Coatings Technology, 2001, 146—147: 537—543.

作者简介：夏卫生，男，1979 年出生，博士。研究领域为机器人等离子熔射成形智能控制、功能涂层、固体氧化物燃料电池制备与性能分析。发表论文 10 余篇。

Email：xiatianhust@hotmail.com

experimental results can validate the current model and shows that the material flows and temperature distributions can be predicted precisely. From the research on material flows around the welding tool, the formation of weld fash in friction stir welding is explained. The 3D material flow patterns on different thicknesses are studied, which is compared with the 2D case to show that the material flows obtained in 2D numerical simulation correspond to the ones near the bottom surface obtained in 3D simulation. The equivalent plastic strain distribution also shows that the shoulder can affect the material behaviors near the top surface and the effect of the shoulder becomes weaker near the bottom surface, which demonstrates that the 2D case correspond to the part near the bottom surface in 3D case.

Key words: friction stir welding; fully coupled thermo-mechanical model; material flow patterns; finite element method

Electrode arc equation and thermodynamic analysis of submerged arc welding with constant current power supply LIU Chaoying[1], HUANG Shisheng[2] (1. Faculty of Electronic Information and Mechatronic Engineering, Zhaoqing University, Zhaoqing 526061, Guangdong, China; 2. Faculty of Mechanic Engineering, South China University of Technology, Guangzhou 510640, China). p22—24

Abstract: The submerged arc welding (SAW) system consists of an inverted welding power supply with constant current output character, a wire feeder, a welding traveller and a controller. Taking the arc voltage and the setting voltage as input parameters, the controller gives a DC output, which is modulated in pulse width modulation scheme, to drive and adjust the wire feeding speed. A mathematical model related to the welding arc and the wire feeding speed during SAW is established in the form of a first order equation. The model described the balance relation between burning the procedure of the wire in the arc and the feeding of the wire via the wire-feeder. According to thermodynamic analysis of the power supply, molten pool and wire, a scheme for the selection of the wire diameter is obtained, on basis of the diameter of the wire being in proportion to the square root of the welding current. A detailed equation between the wire diameter and the welding current is reported.

Key words: submerged arc welding; dynamic model; thermodynamic analysis; wire diameter

Optimal path modeling for redundant robot based on genetic algorithm LIU Yong[1], Wang Kehong[1], Yang Jingyu[2] (1. Department of Material Science and Engineer, Nanjing University of Science and Technology, Nanjing 210094, China; 2. School of Coputer Science and Fechnology, Nanjing University of Science and Technology, Nanjing 210094, China). p25—28

Abstracts: To solve the optimizing problem of the path planning of robot with eleven degree-of-freedom, a multi-object mathematical model and solution plan has been proposed and analyzed. Using genetic algorithm as optimizing method, a adapive degree function was built. The suitable parameter was obtained through lots of practices. The genetic algorithm procedure was designed and realized. Based on this algorithm, optimizing experiments were carried out based on typical space transversal weld by using under 3 degree-of-freedom gantry and 6 degree-of-freedom robot. Results of experiments indicate that the suitable solution can be quickly found through the algorithm. This algorithm was simulated and also loaded to robot controller to do welding experiments. And the results show that robot joints move steady under the best position of robot placement and good welds have been acquired. It shows this method is correct and feasible.

Key words: redundant welding robot; path planning; genetic algorithm

Heating effect of plasma jet and particle flux in plasma spray XIA Weisheng[1], ZHANG Haiou[2], WANG Guilan[1], YANG Yunzhen[1], ZOU Yang[1] (1. State Key Laboratory of Material Processing and Die & Mould Technology, Huazhong University of Science & Technology, Wuhan 430074, China; 2. State Key Laboratory of Digital Manufacturing and Equipment Technology, Huazhong University of Science & Technology, Wuhan 430074, China). p29—32

Abstract: The length of plasma jet was obtained on the basis of digital image processing and the CCD image gathering system, and heating effect was determined through the temperature rising of a substrate in the unit time by an IR pyrometer. Then comparative experiments of heating effect by plasma jet and particle flux were carried out under different spray distances and lengths of plasma jet to analyze their characteristics. Experimental results show that when the length of plasma jet is shorter than or equal to the spray distance, heating effect is dominated by plasma jet. However, if the length is longer than the spray distance, the heating effect of particle flux becomes more and more obvious, but the case for plasma jet drops rapidly. Therefore, the length of plasma jet, as a characteristic evaluation index, can be adopted to select the reasonable spray distance. This is certified by the patterns and cross-section thickness profiles of deposited coatings under different spray distances.

Key words: plasma spraying; heating effect; plasma jet; particle flux; plasma jet length; spray distance

Fe-based alloy composite coating reinforced by Ti($C_{0.3}N_{0.7}$) particle through laser cladding technology QI Yongtian, ZOU Zengda, QU Shiyao, ZHU Qingjun (School of Materials Science and Engineering, Shandong University, Jinan 250061, China). p33—36

Abstract: A new in-situ synthesis method is carried out to produce Fe-based alloy composite coating reinforced by Ti($C_{0.3}N_{0.7}$) particle on the Q235 mild steel through CO_2 laser cladding technology. X-ray diffraction is used for phase identification in the composite coating. The microstructure of laser cladding layer is analyzed by means of optical microscopy, scanning electron microscopy, and electron probe microscopy analyzer. The microhardness distribution is measured by using microhardness tester. The results show that Ti($C_{0.3}N_{0.7}$) particle is produced by an in-situ metallurgical reaction of TiN particle and graphite powder during laser cladding process. The shape of some Ti($C_{0.3}N_{0.7}$) particle is similar to rhombus, and the others are irregular shape. Size of the fine Ti($C_{0.3}N_{0.7}$) particles is within 0.1—5 μm, and evenly in dispersed the matrix. The micro-